On the Localization of 3D Anatomical Point Landmarks in Medical Imagery Using Multi-Step Differential Approaches

Sönke Frantz, Karl Rohr, and H. Siegfried Stiehl

Universität Hamburg, Fachbereich Informatik, Arbeitsbereich Kognitive Systeme
Vogt-Kölln-Straße 30, D-22527 Hamburg
frantz@informatik.uni-hamburg.de

Abstract. In this paper, we investigate differential approaches for the localization of 3D anatomical point landmarks in 3D medical images. First, we study an existing 2D edge intersection approach for localizing corners and theoretically analyze the localization accuracy of this method for an analytic model of an L-junction. Then, we extend this approach to 3D. We propose two two-step and one three-step procedures for refined localization of 3D point landmarks. For these approaches, we experimentally analyze their localization accuracy for 3D synthetic images. Finally, we investigate the localization of anatomical landmarks of the human brain in 3D MR images. It turns out that the multi-step procedures can considerably improve the localization accuracy of landmarks in comparison to existing single-step approaches.

1 Introduction

The registration of medical images such as MR/CT data and digital atlases is important, e.g., for the planning of neurosurgical interventions and radiotherapy. One possibility of registering two images is a point-based approach (see [2, 10]). For this, prominent points, denoted also as point landmarks, have to be extracted from images.

In this paper, we investigate approaches for the localization of 3D anatomical point landmarks in 3D medical images. We consider such kinds of anatomical features which can be geometrically characterized as tip-like structures. These types of points can be found, for instance, on the ventricular system of the human brain (see the left side of Fig. 3) as well as on other structures in the human brain. Only a few automatic approaches for localizing point landmarks in 3D images have been reported (e.g. [12, 9]). However, these contributions only consider the detection step (see also [5] for a recent experimental study on 2D differential approaches). Here, we investigate two-step and three-step 3D differential approaches for refined localization of point landmarks in 3D images. One advantage of these approaches lies in their computational efficiency and their stability w.r.t. noise since only first order partial derivatives of the images are required.

In the following, we first describe an existing 2D two-step approach [4] for accurately locating prominent points and then theoretically analyze this approach for an analytic model of an L-junction. The result of this investigation serves as a motivation to extend the approach from 2D to 3D. After a description of the resulting 3D approach, we propose two two-step and one three-step procedures for the localization of 3D point landmarks. The localization accuracy of these approaches is then evaluated for 3D synthetic as well as 3D MR images.

2 Two-Step Approach for Localizing 2D Landmarks

2.1 Description of the Approach

Förstner and Gülch introduced in [4] a two-step approach for detecting and localizing corners in 2D images. In the first step, points are detected by applying differential operators (detection step). In the second step, the corner position is located more precisely (2D edge intersection step). Thereby it is assumed that each point in the considered window around a detected point contributes with its intensity gradient to the edges covered by the window. The edges are locally approximated with tangent lines. The intensity gradients are taken as the normals for a representation of the tangent lines in the Hessian normal form. The refined estimation of the corner position is obtained by intersecting these lines using the least-squares-method. The approach has been applied to 2D images representing polyhedral objects as well as to 2D aerial images.

2.2 Analytic Study for an L-junction

The first step (detection step) of the approach from [4] has already been analytically analyzed for an L-junction by Rohr in [8] w.r.t. localization accuracy, and it showed superior performance. Here, we additionally study the localization accuracy of the second step (2D edge intersection) for that structure. The ideal sharp L-junction model has been convolved with a 2D Gaussian blurring function, describing the blur of the imaging system (see [8] for details).

Using the detection operator from [4] for different apertures β yields the *dotted line* on the left side of Fig. 1 (denoted as DET). This line represents the localization error w.r.t. the correct position of the unblurred L-junction. For the analytic computation of the operator responses, the intensity gradient is approximated by a first order expansion, thereby assuming an operator size of 3×3 pixels. Application of the 2D edge intersection approach yields the *dashed line* on the left side of Fig. 1. Here we used a window of 3×3 pixels. By successively enlarging the window, one can reduce the localization error to nearly zero when using a window size of 15×15 pixels (right side of Fig. 1).

In summary, our study shows for an L-junction which is a tip-like structure that additionally applying the 2D edge intersection approach can considerably improve the localization accuracy in comparison to applying only the detection operator. These results motivate an extension to 3D which is described next.
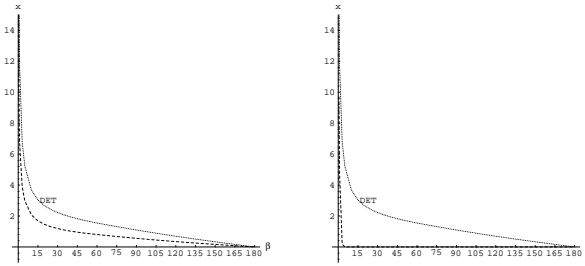
Fig. 1. Theoretic localization accuracy using the 2D edge intersection approach (dashed line) for the L-junction as a function of the aperture β: for window sizes 3×3 pixels (left), 15×15 pixels (right)

3 Extension of the Edge Intersection Approach to 3D

Let us consider the tips of the ventricle system in the human brain (see the black dots within the dashed circles) on the left side of Fig. 3. A simplified model for these tips is a tetrahedron, smoothed with a Gaussian filter. By keeping this simplification in mind, we can apply a 3D extension of the 2D edge intersection approach from [4] for the localization of the tips in 3D medical images.

Let us now extend the approach to 3D. The tip of a tetrahedron can be characterized as the intersection point of three 3D edges. Note, that edges in 3D in general represent surfaces and for the tetrahedron we have plane segments as edges. The 3D edges can be locally approximated with tangent planes. For a suitable window covering sufficient information of the structure, we can intersect the tangent planes (3D edges) to obtain the searched landmark point $\mathbf{x}^*$. The planes are represented in the Hessian normal form, taking the intensity gradients as the normals (cf. the 2D case in Section 2.1). Intersection of the planes with the least-squares-method yields the following system of normal equations

$$\underbrace{\begin{pmatrix} \sum_i g_{x_i}^2 & \sum_i g_{x_i} g_{y_i} & \sum_i g_{x_i} g_{z_i} \\ \sum_i g_{x_i} g_{y_i} & \sum_i g_{y_i}^2 & \sum_i g_{y_i} g_{z_i} \\ \sum_i g_{x_i} g_{z_i} & \sum_i g_{y_i} g_{z_i} & \sum_i g_{z_i}^2 \end{pmatrix}}_{\mathbf{N}} \mathbf{x}^* = \begin{pmatrix} \sum_i g_{x_i}^2 x_i + \sum_i g_{x_i} g_{y_i} y_i + \sum_i g_{x_i} g_{z_i} z_i \\ \sum_i g_{x_i} g_{y_i} x_i + \sum_i g_{y_i}^2 y_i + \sum_i g_{y_i} g_{z_i} z_i \\ \sum_i g_{x_i} g_{z_i} x_i + \sum_i g_{y_i} g_{z_i} y_i + \sum_i g_{z_i}^2 z_i \end{pmatrix} \quad (1)$$

where the index i addresses all points in the considered window and the subscripts to the intensity function $g(x, y, z)$ stand for the partial derivatives in the respective spatial directions. However, solving the former system of equations assumes that we have already selected a suitable region, or, in other words, we first have to detect 3D point landmarks.

4 Detection of 3D Point Landmarks

The covariance matrix of the estimation $\mathbf{x}^*$ for the 3D edge intersection point, obtained by solving Eq. 1, is $\sigma_\varepsilon^2 \mathbf{N}^{-1}$, where $\mathbf{N}$ represents the averaged dyadic gradient product. The factor σ_ε^2 is the estimated variance of the residuals (cf. [6, 4]).

Under the assumption of a normally distributed location, the uncertainty of the estimation is represented by the covariance ellipsoid. Prominent points are characterized by an isotropic and small-sized ellipsoid. These two criteria can be inspected by exploiting the Eigenvalues of $\mathbf{N}$, or, alternatively, by using the determinant $\det(\cdot)$ and the trace$(\cdot)$ of that matrix. Based on $\det(\mathbf{N})$ and trace$(\mathbf{N})$ we can define different 3D extensions of the 2D operators from [4] and [7]: $V^1 = \det(\mathbf{N})/\text{trace}(\mathbf{N})$, $V^2 = \det(\mathbf{N})/\text{trace}(\mathbf{N}^{\#})$ where $\mathbf{N}^{\#}$ denotes the adjunct of the matrix $\mathbf{N}$, and $V^3 = \det(\mathbf{N})$. First experimental results with these 3D detection operators have been reported in [9, 10].

5 Two-Step and Three-Step Procedures for the Localization of 3D Point Landmarks

Based on the 3D extensions described above, we here propose three approaches for the refined localization of landmarks in 3D imagery.

i) Two-step procedure:
First, one of the operators V^1, V^2, or V^3 is applied to the 3D image. The partial derivatives for computing the operator responses are estimated with relative large operators for reasons of robustness w.r.t. noise. In the second step, small-scale operators are used to compute the operator response. This approach is analogous to the 2D procedures investigated in [3, 7] for localizing corners.

ii) Two-step procedure:
This scheme essentially is the 3D extension of the two-step approach of Förstner and Gülch [4]. In our case, first, one of the operators V^1, V^2, or V^3 is applied to detect points. Second, the 3D edge intersection point is computed as described in Section 3, yielding a point with subvoxel accuracy.

iii) Three-step procedure:
This procedure is a combination of the procedures i) and ii) and is therefore a three-step procedure. First, one of the detection operators V^1, V^2, or V^3 is applied. Second, the detected position is refined using small-scale operators for estimating the partial derivatives of the image. In the third step, we start from this refined position and apply the 3D edge intersection approach.

6 Experimental Results for 3D Images

In the following, we present experimental results for 3D synthetic as well as 3D MR images. The experiments have been carried out in the KHOROS environment. For estimating the partial derivatives of the image we have used 3D extensions of the 2D operators by Beaudet [1]. For the detection step, we chose the operator size $5 \times 5 \times 5$ voxels. For the refinement step of the approaches i) and iii), operators of size $3 \times 3 \times 3$ are used. Another free parameter of the operators V^1, V^2, and V^3 which exploit the matrix $\mathbf{N}$ is the width w of the window in which the sums of the matrix elements are computed, i.e. the area of averaging the dyadic gradient product. Here, we chose different values for w,

starting with $w = 3$ which stands for a window size of $3 \times 3 \times 3$ voxels. Operator maxima of V^1, V^2, and V^3 are detected by a local maximum search in a region of $3 \times 3 \times 3$ voxels. In the case of several maxima we have taken the point with the largest operator response.

6.1 3D Synthetic Images

We have investigated the localization accuracy of the approaches i), ii), and iii) for a 3D tetrahedron. The sharpness of the tetrahedron is determined by the aperture β. One can imagine this structure as a 3D generalization of an L-junction with the aperture β within the xy-plane. For the construction of the 3D object, the symmetry line is spread in the direction of the z-axis, enclosing the aperture β with the x-axis.
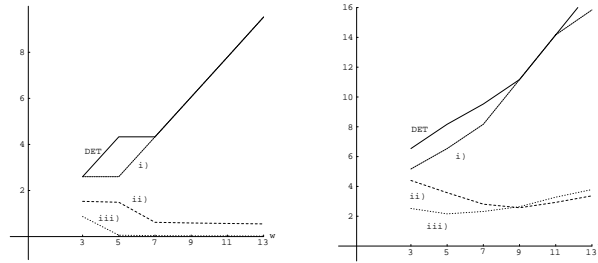

Fig. 2. Localization accuracy as a function of the window width w for a 3D tetrahedron: with $\beta = 90°$ (left) and $\beta = 45°$ (right)

On the left side of Fig. 2, the Euclidean distances of the localized positions to the tip of the tetrahedron with $\beta = 90°$ are plotted as a function of w. Here, DET denotes the detection step using operator V^1. Enlarging this window makes the localization accuracy for DET and i) worse. Conversely, the localization error significantly decreases for the approaches ii) and iii), taking more information of the intensity structure for the computation of the landmark point into account. On the right side of Fig. 2, the improvement of the approaches ii) and iii) in comparison to DET and i) for $\beta = 45°$ is also significant. However, for ii) and iii) and larger windows the error slightly increases. This effect is probably due to discretization errors. In summary, the procedures with 3D edge intersection greatly increase the localization accuracy w.r.t. DET whereas approach i) only hardly improves the result. The results agree with our 2D study above.

6.2 3D Medical Images

In this section, we investigate a 3D MR dataset of the human head. We consider as anatomical landmarks the tips of the frontal, occipital, and temporal horns of the ventricles, abbreviated with MC6, MC7, and MC13, respectively (left
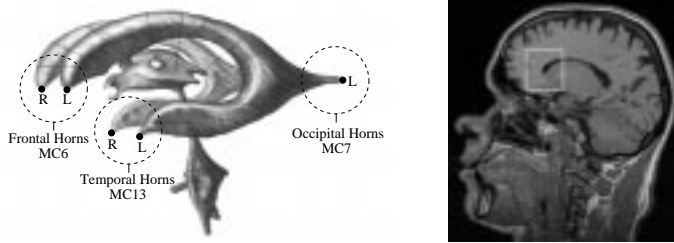
Fig. 3. Ventricular system of the human brain, anatomical preparate (from [11]) (left); sagittal slice of a MR tomogram with the left ventricle (right)

side of Fig. 3). The letters L and R stand for the respective hemispheric parts of the ventricular system. We have manually specified the positions of these landmarks in the investigated datasets and have taken them as ground truth positions, although we know that manual localization of 3D landmarks generally is difficult and may be prone to error. The computation was restricted to a region-of-interest (ROI) with $21 \times 21 \times 21$ voxels. The ROI was centered at the manually specified landmark position. The here considered MR dataset consists of 235 sagittal slices of 256×256 voxels. The resolution was about $1 \times 1 \times 1$mm.

LM/w	DET	i)	ii)	iii)	LM/w	DET	i)	ii)	iii)
MC6L/3	1, 2, 0 2.24	0, 1, 0 1.00	0.08, 1.50, 0.85 1.73	0.79, 0.27, 0.36 0.91	MC6R/3	1, 2, 0 2.24	1, 1, 0 1.41	0.03, 1.50, 0.13 1.51	0.30, 0.21, 0.52 0.63
MC6L/5	1, 2, 0 2.24	1, 1, 0 1.41	0.91, 0.43, 1.16 1.54	0.91, 0.59, 1.00 1.47	MC6R/5	1, 2, 0 2.24	1, 2, 0 2.24	0.84, 0.90, 0.76 1.45	1.44, 0.23, 1.27 1.93
MC7L/3	4, 5, 1 6.48	3, 6, 1 6.78	2.52, 6.19, 1.12 6.78	0.82, 7.46, 0.48 7.52	MC7R/3	3, 2, 0 3.61	2, 1, 0 2.24	1.80, 1.58, 0.14 2.40	0.62, 0.52, 0.15 0.82
MC7L/5	3, 2, 2 4.12	2, 1, 1 2.45	0.53, 0.96, 1.51 1.86	0.52, 0.15, 0.86 1.02	MC7R/5	3, 2, 0 3.61	3, 2, 0 3.61	0.75, 0.61, 0.82 1.27	0.28, 0.03, 0.89 0.93
MC13L/3	1, 2, 0 2.24	1, 1, 1 1.73	0.79, 1.88, 0.86 2.21	0.56, 0.06, 3.31 3.36	MC13R/3	0, 1, 2 2.24	0, 1, 1 1.41	0.91, 0.41, 0.87 1.33	0.72, 0.61, 1.31 1.61
MC13L/5	2, 2, 1 3.00	2, 2, 1 3.00	0.92, 1.21, 0.88 1.76	0.59, 0.95, 0.55 1.25	MC13R/5	1, 1, 5 5.20	1, 1, 4 4.24	0.60, 0.30, 5.67 5.71	1.51, 0.75, 2.68 3.17

Table 1. Localization results for MR data: left ventricle (left), right ventricle (right)

In Tab. 1, the results for the left and right ventricles are reported, respectively. The first column gives the considered landmark (LM) and the width of the window for averaging the dyadic gradient product (w). Then follow the respective localized positions for the detection step (DET) and the approaches i), ii), and iii). All positions are relative w.r.t. the manually specified landmark positions (top row of a box). Additionally, we computed the Euclidean distances to the manually specified landmark positions (bottom row of a box). The refined localization i) with small-scale operators yields an improvement in the mean of about 0.7 voxels w.r.t. DET. Edge intersection ii) decreases the error for about 0.8 voxels w.r.t. DET. For approach iii), the error can be decreased further for about 0.6 voxels w.r.t. i). Thus, we obtain an overall improvement of about 1.2 voxels for approach iii). In most cases the approaches ii) and iii)

yielded the best results. The relative large errors for the right temporal horn are conspicuous. One reason for this might be the uncertainty induced by the manual landmark specification which is very difficult for this landmark. We notice that at the tip of the left occipital horn are two salient curvature extrema. The point more far away from the manually specified position was localized for $w = 3$. In general, the localization accuracy gets worse when we enlarge the window for the computation of $\mathbf{N}$ which is what we expect. We have also applied these approaches to other medical images yielding similar results.

In Fig. 4, the localized point at the tip of the frontal horn is visualized in three orthogonal image intersections. For visualization purposes, the point coordinates obtained from ii) and iii) have been rounded to voxel coordinates. The location of that structure within the human brain is marked by a square (sagittal view on the right ride of Fig. 3).
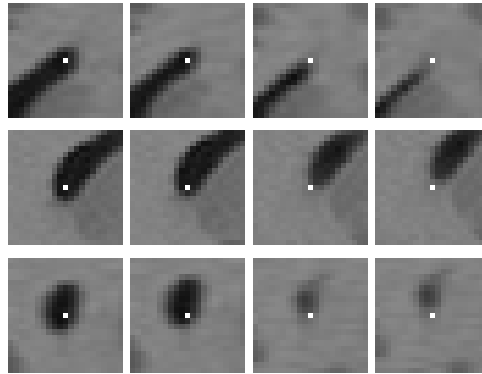

Fig. 4. Localized points at the tip of the left frontal horn; approaches DET, i), ii), and iii) (from left to right), axial, sagittal, and coronal view (from top to bottom)

7   Summary

We have investigated multi-step differential approaches for refined localization of 3D point landmarks. The promising results due to our theoretical study of the 2D edge intersection approach motivated an extension to 3D. Based on the 3D extension of this approach, we proposed two two-step and one three-step procedures for the localization of 3D point landmarks, combining detection and 3D edge intersection. We have experimentally investigated these approaches for 3D synthetic as well as 3D MR images. For synthetic data, the combination of a two-step procedure of large-scale and small-scale differential operators followed by the edge intersection approach, i.e. the three-step procedure, yielded the most precise results. For MR data, the two-step and three-step procedures, both including 3D edge intersection, yielded the best results. In comparison to a single-

step procedure for locating point landmarks by means of applying differential operators, the localization accuracy has been significantly improved.

Acknowledgement

References

1. P. R. Beaudet. Rotationally invariant image operators. In *Proc. Intern. Conf. Pattern Recognition*, pages 579–583, Kyoto, Japan, November 1978.
2. F. L. Bookstein. Principal Warps: Thin-Plate Splines and the Decomposition of Deformations. *IEEE Transactions On Pattern Analysis And Machine Intelligence*, 11(6):567–585, June 1989.
3. L. Dreschler. *Ermittlung markanter Punkte auf den Bildern bewegter Objekte und Berechnung einer 3D-Beschreibung auf dieser Grundlage*. Dissertation. Fachbereich Informatik, Universität Hamburg, 1981.
4. W. Förstner and E. Gülch. A Fast Operator for Detection and Precise Location of Distinct Points, Corners and Centres of Circular Features. In *Proc. of Intercommission Conference on Fast Processing on Photogrammetric Data*, pages 281–305, Interlaken, Switzerland, June 1987. ISPRS Intercommission Workshop.
5. T. Hartkens, K. Rohr, and H. S. Stiehl. Evaluierung von Differentialoperatoren zur Detektion charakteristischer Punkte in tomographischen Bildern. In B. Jähne, P. Geißler, H. Haußecker, and F. Hering, editors, *18. DAGM-Symposium Mustererkennung*, Informatik aktuell, pages 637–644. Springer-Verlag Berlin Heidelberg, September 1996.
6. D. F. Morrison. *Multivariate Statistical Methods*. McGraw-Hill Book Company, New York, NY, USA, 1967.
7. K. Rohr. *Untersuchung von grauwertabhängigen Transformationen zur Ermittlung des optischen Flusses in Bildfolgen*. Diplomarbeit. Institut für Nachrichtensysteme, Fakultät für Elektrotechnik, Universität Karlsruhe, November 1987.
8. K. Rohr. Localization Properties of Direct Corner Detectors. *Journal of Mathematical Imaging and Vision*, 4:139–150, May 1994.
9. K. Rohr. On 3D Differential Operators for Detecting Point Landmarks. *Image and Vision Computing*, 15:219–233, 1997.
10. K. Rohr, H. S. Stiehl, R. Sprengel, W. Beil, T. M. Buzug, J. Weese, and M. H. Kuhn. Point-Based Elastic Registration of Medical Image Data Using Approximating Thin-Plate Splines. In K.-H. Höhne and R. Kikinis, editors, *Proc. 4th Intern. Conf. Visualization in Biomedical Computing (VBC'96)*, Lecture Notes in Computer Science No. 1131, pages 297–306, Hamburg, Germany, September 1996. Springer-Verlag.
11. J. Sobotta. *Atlas der Anatomie des Menschen*. Urban & Schwarzenberg, München, 19 edition, 1988.
12. J.-P. Thirion. Extremal Points: Definition and Application to 3D Image Registration. In *Proc. IEEE Computer Society Conference on Computer Vision and Pattern Recognition 1994 (CVPR '94)*, pages 587–592, Seattle, WA, USA, June 1994. IEEE Computer Society Press.